# Contributions to an Ultra-High Temperature (250 °C/500 °F) Bearingless Pump

T. Wellerdieck,
P. Peralta,
T. Nussbaumer,
J. W. Kolar

# Contributions to an Ultra-High Temperature (250 °C/500 °F) Bearingless Pump

T. Wellerdieck[1], P. Peralta[1], T. Nussbaumer[2], J.W. Kolar[1]
[1] Power Electronic Systems Laboratory, Federal Institute of Technology
Zurich, Switzerland
[2]Levitronix GmbH, Zurich, Switzerland
E-mail: wellerdieck@lem.ee.ethz.ch

*Abstract*—The semiconductor industry demands for pumps which handle aggressive fluids at very high temperatures, as this is an important step towards higher process speeds and increased yield in semiconductor etching applications.

This paper presents the thermal, electrical and mechanical design of a bearingless pump for operating temperatures of up to 250 °C without active cooling. A detailed thermal analysis of the machine is presented which allows for the prediction of the thermal stress of critical components. The machine design is based on the prediction of the internal temperatures and hydraulic specifications of the pump. Furthermore, a hallsensorless, observer-based, control of the rotor angle is presented. The necessity for this control scheme arises from the high temperatures that prevent the usage of conventional angle measurement systems.

*Index Terms*—bearingless disk motor, permanent magnet motor, high temperature, sensorless control.

Fig. 1: CAD rendering (a) and photography (b) of the bearingless ultra-high temperature pump.

## I. Introduction

In this paper an ultra-high temperature (UHT) centrifugal pump with magnetically levitated rotor is proposed. The pump is specified to handle agressive fluids at temperatures of up to 250 °C. Table I lists the most important specifications of the pump system. The drive is implemented as a permanent magnet synchronous machine (PMSM) with a one polepair rotor and a three phase stator [1]. The rotor magnet is ring-shaped with a diameter that exceeds its height. Thus, the machine can be referred to as a bearingless disc drive [2]. The machine is implemented as an inrunner. The disk shape results in a passive axial and tilting stability [3]. Therefore, the bearing only needs to stabilize the rotor in radial direction. Figure 1(a) shows a CAD rendering, illustrating the temple design of the stator, which is chosen to limit the radial dimension of the pump housing. A photograph of the prototype is shown in Fig. 1(b).

This paper describes some challenges that have to be overcome in order to operate a bearingless machine in agressive, high temperature environments. The most important design steps are the approximation of the internal machine temperatures, the selection of suitable components and the control of such a machine. The insights gained from the design of the UHT-pump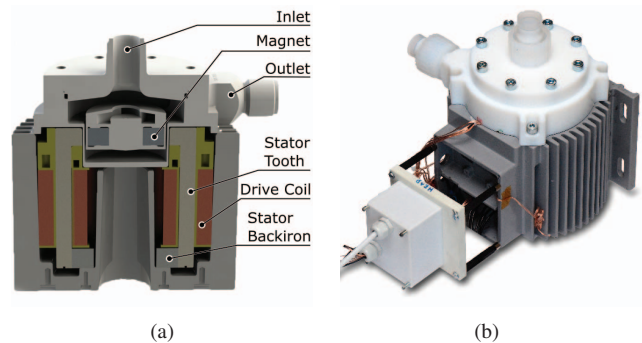 can be used for any bearingless machine that operates at high internal temperatures, be it due to external heating or high power densities. The UHT-pump was designed with a focus on applications in the semiconductor industry. The following passage describes those applications in detail.

| | Value | Units |
|---|---|---|
| Maximal Fluid Temperature | 250 | °C |
| Maximal Flow | 120 | $l \cdot min^{-1}$ |
| Maximal Pressure | 412 | kPa |
| Rotational Speed | 8000 | RPM |
| Maximum Input Power | 2000 | W |
| Input Voltage | $200 - 240$ | $V_{RMS}$ |

TABLE I: Overview of ultra-high temperature pump specifications.

The lithographic fabrication of a semiconductor wafer is divided into multiple process steps. Different chemical and physical procedures are perfomed on the substrate material in order to manufacture the desired structures. First the wafer is cleaned and prepared for the process. Subsequently, the substrate is coated with a photoresistive film. After prebaking, specific areas of the film are developed by means of exposure to light, where the exposed area is defined by the shape of the photomask. This is followed by the development of the photoresist and additional baking. Once the photoresist is fully cured, its patterns have to be transfered to the substrate. This

includes removal of substrate by means of etching, addition of material by means of material deposition, or doping of the substrate with ions. The remaining photoresistive film is removed once the transfer process is completed. This process, referred to as stripping, is usually done by ashing the photoresist by use of a high temperature plasma, called dry stripping, and a subsequent removal of the ashed photoresist by the use of liquid chemicals, called wet stripping. After the photoresist is removed, the substrate is cleaned again and the process can be started over again to apply the next strucure to the substrate [4].

During the wet stripping process agressive acids, e.g. sulfuric acid ($H_2SO_4$), are used to remove the photoresistive layer. The depletion rate of the photoresistive layer is exponentially dependent on the temperature of the acid and approximately doubles if the acid is heated by 10 °C. Furthermore, it is dependent on the concentration of the acid. An exclusive, refered to as full, wet stripping, without the need for dry stripping, can be achieved if the acid temperature is sufficiently high. This can be accomplished by heating $H_2SO_4$ from 150 °C to 200 °C through an exothermic reacion on the wafer [5], [6]. The temperature on the wafer can be further increased if the initial temperature of the $H_2SO_4$ is raised. Therefore, a possibility to handle concentrated sulfuric acid at very high temperatures while ensuring extremely low contamination is desireable. The latter is critical since the level of contamination has a direct impact on the yield of production and thus on the manufacturing cost [4]. Therefore, the semiconductor manufacturing process is conducted in sealed containments and only ultra-pure process fluids are used.

Low contamination requires the handling of the acids with materials that do not react with the chemicals used in the stripping and etching processes. The only materials suitable for $H_2SO_4$ above 200 °C are fluorpolymers such as polytetrafluoroethylene (PTFE) and perfluoroalkoxy polymer (PFA). Bellows pumps that use these materials are available for fluid temperatures of up to 210 °C, [7]. These pumps consist of a PTFE bellow that is cyclically compressed and expanded, yielding a pulsating fluid flow. The plastic material of the bellow is exposed to significant mechanical stress and thus has a limited lifetime even at tempeartures significantly below the maximum operation temperature of PTFE of 260 °C.

This paper proposes the useage of a pump that is based on a bearingless design instead of a bellows pump. The materials in contact with the fluid are fluorpolymers but the bearingless drive ensures smaller mechanical stress. This allows the useage of PTFE and PFA up to their rated temperatures without sacrificing reliability or life expectancy.

Low contamination levels are achieved as there is no deformation of the materials or abrasive friction. The fluid handling compartement is completely closed. There is no need for seals since no shaft has to be driven externally.

This paper is structed as follows: In Section II it is shown how to approximate torque, speed and power requirements for the pump based on its flow and pressure specifications. A way to analyze the temperature transport inside the pump is presented in Section III, yielding a temperature distribution. The machine design is derived from these requirements as described in Section IV. A sensorless approach for detecting the rotor angle is presented in Section V.

## II. PUMP SPECIFICATIONS

### A. System Description

The UHT-pump is based on a commercially available single tab centrifugal pump by *Levitronix*. The UHT-pump is required to have similar pressure and flow as the commercial product at temperatures of up to 250 °C. The rated operating point is defined for $H_2SO_4$ with a flow of $Q = 70 \frac{1}{\min}$ and a pressure difference of $\Delta p = 300$ kPa. This lies well inside the maximal ratings as listed in Tab. I.



Fig. 2: $QH$ curves for the pumphead and impeller of the pump.

### B. Hydraulic Specifications

The performance of the active hydraulic elements, specifically the pumphead and the impeller, were measured with water at room temperature. The rated pressure and the density of the fluid define the hydraulic head $H$. Head and hydraulic flow $Q$ are used to determine the nominal speed based on the measured $QH$ curves cf. Fig. 2.

The head is calculated as

$$H = \frac{\Delta p}{\rho \cdot g} \qquad (1)$$

with $\Delta p$ being the pressure difference between pump outlet and pump inlet and $\rho$ being the fluid density. The density of $H_2SO_4$ is $1840 \, \frac{kg}{m^3}$ at room temperature. At different temperatures the density $\rho$ can be calculated as

$$\rho_{\vartheta_2} = \frac{\rho_{\vartheta_1}}{1 + \beta \left( \vartheta_1 - \vartheta_2 \right)} \tag{2}$$

for the temperatures $\vartheta_1$ and $\vartheta_2$ and the thermal coefficient of thermal expansion $\beta$. At 250 °C the density is $1452 \, \frac{kg}{m^3}$. This allows for the calculation of the hydraulic head at both temperatures

$$\begin{aligned} H_{\text{hydr,RT}} &= \frac{\Delta p}{\rho_{\text{RT}} \cdot g} = 16.62 \text{ m} \\ H_{\text{hydr,250 °C}} &= \frac{\Delta p}{\rho_{250 \text{ °C}} \cdot g} = 20.96 \text{ m} \end{aligned} \tag{3}$$

which shows that the maximum head is required for pumping the hot sulfuric acid. Based on the $QH$ measurements a rated speed of 6500 RPM can be found. The hydraulic power during rated operation is

$$P_{\text{hyd}} = \Delta p \cdot Q = 350 \text{ W}. \tag{4}$$

The rated torque can be calculated using the power ballance and the hydraulic efficiency of the impeller. The efficiency is again measured with water at room temperature at a given head and flow. The required torque is

$$T_{\text{el}} = \frac{P_{\text{hyd}}}{\omega \eta} = 1.66 \text{ Nm}. \tag{5}$$

Thus, the machine design must aim to achieve a torque of 1.66 Nm at a speed of 6500 RPM while ensuring the bearing stability of the machine.

## III. THERMAL MODEL

### A. Thermal Modelling

The aim of the thermal model is to give an approximation of the expected temperature at the windings. The model is based on a lumped parameter-based analysis [8]. Heat transfer by means of conduction, convection and radiation is considered in the model.

### B. Conductive Heat Transfer

A thermal resistance describing the conductive heat transfer in one direction is

$$R_{\text{th}} = \frac{L}{\lambda \cdot A} \tag{6}$$

with the length and the area of the conductive body $L$ and $A$, respectively, and the thermal conductivity $\lambda$. The thermal conductivity is assumed to be constant over the temperature range of interest. The length and area of the conductive body change with temperature due to thermal expansion.

### C. Convective Heat Transfer

Heat from the pump case surface is transfered to the ambiance by means of natural convection. The pump is oriented as shown in Fig. 1(a). The case surface is split into a flat part and a part with cooling fins. The thermal resistance describing the flat surface is calculated under the assumption that the boundary layer of the flow is small in comparison of the cylinder diameter. The convective heat transfer is thus described by the formula for a flat vertical surface. The thermal resistance can be calculated as

$$Gr = \frac{gH^3 \beta \Delta\vartheta}{\nu^2}, \quad Ra = Gr \cdot Pr$$

$$Nu = \left( 0.825 + \frac{0.387 Ra^{1/6}}{\left( 1 + \left( \frac{0.492}{Pr} \right)^{9/16} \right)^{8/27}} \right)^2 \tag{7}$$

$$\alpha = \frac{Nu \cdot \lambda}{H}, \quad R_{\text{th,S}} = \frac{1}{H\pi D\alpha}$$

with the case diameter $D$, height $H$, the difference between case and ambient temperature $\Delta\vartheta$, the Prandtl number $Pr$ and the kinematic viscosity of air $\nu$. The parameter $\beta$ is calculated using the case temperature as $\beta = \frac{1}{\vartheta_{\text{case}}}$.

The heat transfer from the case surface with fins is calculated for each fin channel. A fin channel is the volume between two adjacent fins. It is assumed that the flow in one fin channel does not affect the flow in the others. The thermal resistance of such a channel can be calculated as

$$Gr = \frac{g\beta\Delta\vartheta s^4}{\nu^2 H}, \quad Ra = Gr \cdot Pr$$

$$Nu \approx \left( \frac{1}{(1/3 \cdot Ra)^{3/2}} + \frac{1}{\left( 0.69 \left( Ra \right)^{1/4} \right)^{3/2}} \right)^{-2/3} \tag{8}$$

$$\alpha = \frac{Nu \times \lambda}{s}, \quad R_{\text{th,F}} = \frac{1}{\alpha A_{\text{ch}}}$$

with $s$ being one half of the spacing between two adjacent fins and $A_{\text{ch}}$ denoting the surface area of the case covered by fins. Equation 8 can be simplified if the flow is known to either be laminar or turbulent. The total convective heat transfer from the case to the ambiance is described by:

$$R_{\text{th}} = \left( \frac{1}{R_{\text{th,S}}} + \frac{1}{R_{\text{th,F}}} \right)^{-1} \tag{9}$$

The derivations of (7) and (8) can be found in [9].

### D. Radiative Heat Transfer

Heat is also transported from the case surface to the ambiance by means of radiation. The thermal resistance for the radiation is:

$$R_{\text{th}} \approx \frac{T_c - T_A}{\epsilon\sigma A \left( T_c^4 - T_A^4 \right)} \tag{10}$$

with the case surce $A$, the emissivity $\epsilon$ and the Boltzman constant $\sigma$.

### E. Modelling of the Machine Winding

The winding number was set to 231 turns for the thermal model. The wire is wound in 7 layers with 33 turns each. The average temperature of each turn was evaluated. The thermal conductivity from turn to turn was calculated as shown in [10].

### F. Machine Losses

The machine is heated by internal losses. The losses can be divided into copper and iron losses. The copper losses generated in turn $i$ of the winding are

$$P_{\mathrm{Cu,i}} = \rho_{\mathrm{Cu,RT}} \left(1 + \alpha_{\mathrm{Cu}} \left(\Delta\vartheta_{\mathrm{i}}\right)\right) \frac{l_{\mathrm{turn,i}}}{A_{\mathrm{cu}}} I_{\mathrm{D}}^2 \qquad (11)$$

where $\rho_{\mathrm{Cu,RT}}$ is the resistivity at room temperature, $\alpha_{\mathrm{Cu}}$ is the thermal coefficient of the resistivity, $\Delta\vartheta_{\mathrm{i}}$ is the temperature difference between the wire- and room temperature, $l_{\mathrm{turn,i}}$ is the wire length of the turn, $A_{\mathrm{Cu}}$ is the copper wire cross section and $I_{\mathrm{D}}$ is the drive current. The copper losses for each turn are calulated since turns on the inner layer are shorter and thus create less loss than the turns on the outer layers. The temperature of each layer is also different. Layers in the middle of the winding tend to be hotter than layers on the surface. The total copper losses per winding are

$$P_{\mathrm{Cu}} = \sum_{i} P_{\mathrm{Cu,i}}. \qquad (12)$$

The iron losses can be divided into hysteresis losses and eddy current losses. The hysteresis losses are approximated by

$$P_{\mathrm{Hy}} = c_{\mathrm{Hy}} f \hat{B}^{1.6} \rho_{\mathrm{Fe}} V_{\mathrm{Fe}} \qquad (13)$$

with $c_{\mathrm{Hy}}$ being a known constant for the stator material, $f$ being the electric frequency, $\delta_{\mathrm{Fe}}$ being the density of iron and $V_{\mathrm{Fe}}$ being the volume of the stator iron. The amplitude $\hat{B}$ was calculated using FEM methods. The eddy current losses can be approximated with

$$P_{\mathrm{Ed}} = c_{\mathrm{ed}} f^2 \hat{B}^2 d_{\mathrm{Fe}}^2 \rho_{\mathrm{Fe}} V_{\mathrm{Fe}} \qquad (14)$$

with $c_{\mathrm{ed}}$ being a material constant and $d_{\mathrm{Fe}}$ being the thickness of the sheeting.

The temperature model was evaluated at rated operation. The resulting copper and iron losses were approximately $P_{\mathrm{Cu}} \approx 20$ W and $P_{\mathrm{Fe}} = P_{\mathrm{Hy}} + P_{\mathrm{Ed}} \approx 40$ W, respectively.

### G. Heating from the Fluid

The fluid is assumed to have a fixed temperature of 250 °C. Consequently, the losses of the pump do not change the fluid temperature. Heat is transported from the pumphead to the machine by means of conduction.

### H. Solution of the Thermal Model

The machine is divided into 242 nodes and the temperature is evaluated for each node. Heat flow between the nodes is modelled with the use of a thermal impedance matrix consisting of the thermal resistors. The temperature at each node is used to update the temperature dependent thermal resistors and losses. The solution of the model is performed iteratively.

The highest temperatures in the machine are reached close to the airgap and are in the range of 220°C to 250°C. The temperature at the machine coils is in the range of 170 °C to 210 °C. The average temperature of each turn in the coil is shown in Fig. 3. The outermost layer of the coil is cooled by the case. The coil is heated by internal copper losses and from the top by means of conduction of heat through the pumphead. A temperature hotspot is clearly visible at the windings of the middle layer close to the pumphead. These windings define the minimum temperature rating for the wire of the coils.
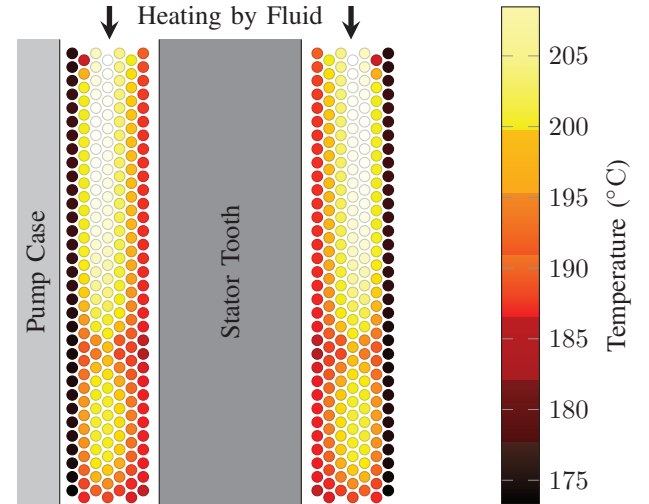


Fig. 3: Average temperatures in each winding according to the thermal model.

## IV. MACHINE DESIGN

### A. Design Process

The design process of the UHT-pump is based on the torque and power requirement as described in Section II and the temperature approximation presented in Section III. An initial machine design, including the magnetic circuit and the windings, can be derived from these specifications. The losses generated with this design are then used to update the interntal machine temperatures and if they exceed the material ratings the machine design must be adapted. Only the final design, including two different wire materials, is shown here.

*B. System Description*

The pump system consists of two components in contact with the fluid, namely the pumphead and the rotor, and a stator which generates the magnetic field in the airgap required to levitate the rotor and generate the torque.

The rotor consists of an impeller and a permanent magnet. The impeller is the active hydraulic element and is mounted onto the rotor magnet. The pumphead and the impeller have to be designed carefully to ensure mechanical stability at 250 °C while providing corrosion resistance.

The stator, consisting of six steel teeth, is made out of sheeted steel to reduce eddy currents. The teeth first extend radially from the airgap and then, after a 90 ° bend, in axial direction, cf. Fig. 1(a). This so-called temple design reduces the outer diameter of the machine. The theeth are connected to each other by means of a stator back iron. The air gap length of the pump is 4.8 mm. The maximum operating temperature of the sheeted iron is well above 250 °C.

*C. Magnet Specifications*

The machine uses a high temperature rare earth magnet. The rotor magnet is ring shaped, radially magnetized and has a polepair number of 1. Ther permanent magnet of the machine has to be designed for operating temperatures of more than 250 °C since it is completely submerged in the hot fluid and cannot be cooled. Any losses generated in the rotor will further increase the magnet temperature.

*D. Winding Wire*

Bearingless machines have long airgap lengths compared to conventional machines. Therefore, it is challenging to achieve a sufficiently high stator flux density in the airgap to achieve the desired torque. Thus, a wire must be chosen that allows for a high windingnumber and a high fillfactor.

The temperature at the windings at rated operation is between 170 °C and 210 °C, c.f. Section III. A 20 % margin was added to this temperature to account for uncertainties in the thermal model. Therefore, the winding wire is designed to withstand 250 °C.

Pure copper experiences accelerated oxidation above 200 °C. The diffusion of oxygen through the insulation material is sufficient to significantly reduce the lifetime of copper wire. The conductor is, therefore, implemented as nickel plated copper wire with a nickel concentration of 27 %. The nickel plating protects the copper conductor from oxidation but also reduces the conductivity to 5.5E7 S/m.

Two nickel clad copper wires with different insulations were best suited for the application at hand. The first wire is insulated with perfluorpolymere material. This wire is available with temperature ratings of 250 °C and 300 °C. The disadvantage of perfluorpolymere insulated wire is its thick insulation resulting in a relatively poor fill factor of 0.5. The second wire is ceramic-insulated wire. Ceramic insulation allows for long-time operation at temperatures of up to 500 °C. The insulation is thin which allows a comparably high fill factor of 0.78. The disadvantage of ceramic wire is that the insulation is prone to cracks and thus care must be taken during assembly of the stator windings.

*E. Electrical Specifications*

The windings are implemented as concentrated windings around the stator teeth. There are two fundamentally different options for integrating drive and bearing in a bearingless machine. The windings for drive and bearing can be wound seperately, resulting in two sets of windings. One set only generates bearing forces and one set only generates torque. Alternatively, only one winding set, producing both bearing forces and torque can be wound. This winding scheme is referred to as combined windings [11].

A seperate winding concept in case of the UHT-pump can be implemented with six bearing coils with currents $I_{B1}, \ldots, I_{B6}$ driven by one three phase system and six drive coils with currents $I_{D1}, \ldots, I_{D6}$ driven by one three phase system. The currents in the windings are

$$
\begin{aligned}
I_{B1} = I_{B4} &= \hat{I}_B \cdot \cos(\phi_B) \\
I_{B2} = I_{B5} &= \hat{I}_B \cdot \cos(\phi_B + 120\ ^\circ) \\
I_{B3} = I_{B6} &= \hat{I}_B \cdot \cos(\phi_B - 120^\circ) \\
I_{D1} = -I_{D4} &= \hat{I}_D \cdot \cos(\phi_D) \\
I_{D2} = -I_{D5} &= \hat{I}_D \cdot \cos(\phi_D + 120\ ^\circ) \\
I_{D3} = -I_{D6} &= \hat{I}_D \cdot \cos(\phi_D - 120^\circ),
\end{aligned}
\tag{15}
$$

with the bearing and drive current amplitudes $\hat{I}_B$ and $\hat{I}_D$ and bearing and drive current angles $\phi_B$ and $\phi_D$. The control of the bearing and the drive are independent.

For the pump presented here, a combined concept with six coils, driven by one six phase system, was chosen. The main advantage of combined coils is the fact that the highest bearing forces are required during start up. Therefore, the start up of the rotor determines the volume of the bearing coils. During operation, when the rotor is levitated, the bearing forces are usually much smaller and this volume could be used for torque generation. With combined coils all the winding volume can be used for force generation during start up and

no bearing volume is wasted during levitation. The currents in the combined coils $I_{C1}, \ldots, I_{C6}$ are a superposition of bearing and drive currents as shown in [12]. The currents are dependent on (15) and can be calculated as

$$
\begin{aligned}
I_{C1} &= I_{B1} + I_{D1} & I_{C4} &= I_{B1} - I_{D1} \\
I_{C2} &= I_{B2} - I_{D3} & I_{C5} &= I_{B2} + I_{D3} \\
I_{C3} &= I_{B3} + I_{D2} & I_{C6} &= I_{B3} - I_{D2}.
\end{aligned} \tag{16}
$$

Figure 4 shows the simulated and measured torque for the machine for a given drive current. The saturation of the iron circuit is clearly visible, but $1.66 \ \text{Nm}$ of torque can be reached, cf. Section II,
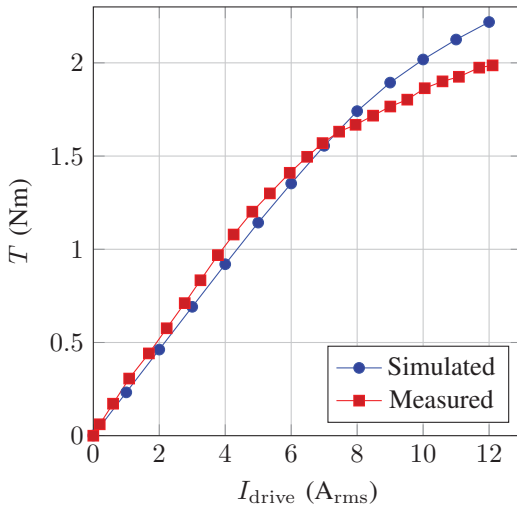


Fig. 4: Torque curves for the ultra-high temperature pump.

## V. HALLSENSORLESS CONTROL

### A. Observer Structure

The angle of the rotor flux must be known in order to efficiently control a PMSM. In case of a bearingless machine the angle is also required to control the bearing. The rotor angle is usually determined by hall sensors which sense the rotor field. These hall sensors have to be mounted sufficiently close to the airgap of the machine. However, the temperatures close to the airgap are in the range of $220 \ °\text{C}$ to $250 \ °\text{C}$ in case of the UHT-pump. Hall sensors with this temperature rating are not commercially available. Therefore, a sensorless angle detection is necessary to drive the pump.

Two bearing observers were designed to obtain an estimation $\hat{\phi}_R$ of the rotor angle $\phi_R$. The first observer, referred to as lowspeed observer, operates during startup and rotational speeds of up to 1500 RPM, similar to [13]. The second observer, referred to as high speed observer, operates from 1500 RPM up to 10000 RPM, which is the maximum speed of the machine.

### B. Lowspeed Observer

*1) Initial Angle Detection:* The rotor angle must be known in order to bring the rotor to levitation. The direction of the rotor magnetization of a one pole pair rotor can be found by using the fact that the rotor always lands with a pole facint the stator. cf. Fig. 5(a). The direction of magnetization can be calculated from the rotor position as

$$
\phi_{\text{mag}} = \arctan \frac{\Delta y_0}{\Delta x_0}, \tag{17}
$$

with the initial displacement from the middle of the stator $\Delta x_0$ and $\Delta y_0$. However, it is unclear which pole is touching the stator. Therefore, the initial rotor angle estimates are

$$
\hat{\phi}_{R,\text{init}} = \begin{cases} \phi_{\text{mag}} \\ \phi_{\text{mag}} + 180 \ °. \end{cases} \tag{18}
$$

The observer assumes that $\hat{\phi}_{R,\text{init}} = \phi_{\text{mag}}$. The bearing is used to check the validity of the guess. The bearing current is limited to a small value and the reference position of the rotor $P_R^*$ is rotated clockwise. If the angle assumption is correct then the rotor will tilt in clockwise direction. If the assumption is incorrect then the rotor will tilt counterclockwise, cf. Fig 5(b). The tilting can be observed by the position sensors. The rotor can be brought to levitation once the the guess of the initial rotor angle $\hat{\phi}_{R,\text{init}}$ is verified.
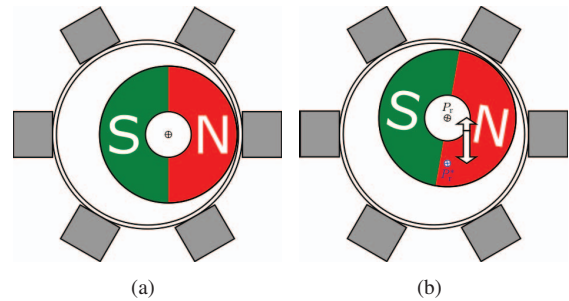


(a)             (b)

Fig. 5: Top view of the landed rotor and the stator back iron (a) and detection of a bad initial angle guess by clockwise rotation of reference position and counterclockwise tilting of rotor (b).

*2) Lowspeed Angle Control:* For low speeds the rotor angle is controlled by means of feed forward control. A one polepair field is generated by the stator. The field is generated by applying a current with amplitude $I_D$ and angle $\phi_D$. The initial value for the stator field angle is

$$
\phi_D = \hat{\phi}_{R,\text{init}} + 180 \ °. \tag{19}
$$

If the stator field is rotated by changing $\phi_D$, then the rotor will follow, that is

$$
\phi_R = \phi_D + \Delta\phi \tag{20}
$$

with the angle difference $\Delta\phi$. The estimated rotor angle is set to $\hat{\phi}_\mathrm{R} = \phi_\mathrm{D} + 180\,°$. The torque acting on the rotor is

$$T_\mathrm{m} \propto I_\mathrm{D} \cdot \sin(\Delta\phi). \tag{21}$$

Therefore, the maximum torque during low speed operation is limited by the fact that the bearing requires a reasonably small estimate error to work properly. In a pump this is acceptable since the torque scales with

$$T_\mathrm{load} \propto n^2, \tag{22}$$

$n$ being the rotational speed. Thus, the load torque acting upon the rotor is less than $5\,\%$ of the rated torque if the low speed observer is used up to 1500 RPM.

*3) High Speed Observer:* The rotor angle of a PMSM can be dermined based on the estimation of the induced voltage of the spinning rotor. The induced voltage and, subsequently, the stator flux $\underline{\Psi}_\mathrm{S}$ and the rotor flux $\underline{\Psi}_\mathrm{R}$ can be derived from measurements of the terminal voltage $\underline{u}_\mathrm{S}$ and stator current $\underline{i}_\mathrm{S}$ by

$$\begin{aligned} \underline{\Psi}_\mathrm{S} &= \int (\underline{u}_\mathrm{S} - R_\mathrm{S}\underline{i}_\mathrm{S})\, dt \\ \underline{\Psi}_\mathrm{R} &= \underline{\Psi}_\mathrm{S} - \underline{i}_\mathrm{S} L_\mathrm{S} \end{aligned} \tag{23}$$

with the resistance of the machine winding $R_\mathrm{s}$ and the stator inductance $L_\mathrm{S}$.

The rotor angle can be directly calculated from the rotor flux. Alternatively, a feedback solution with a phase locked loop (PLL) is used. This observer only works if the magnitude of the induced voltage is significantly higher than any measurement noise. A minimum machine speed is, therefore, required to guarantee a good observer performance.
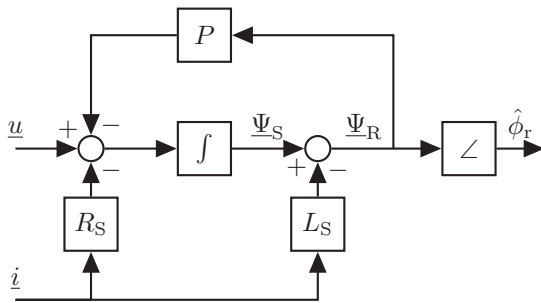


Fig. 6: Control block diagram of the rotor angle estimation with flux feedback to remove DC offsets.

One problem with the open integration, as shown in (23), is that any DC error in the current measurement will drive the integration into saturation. Therefore, an integrator with flux feedback, as shown in Fig. 6, is used to prevent saturation.

The resulting high speed observer is robust to torque and force changes during operation. However, the temperature of the machine winding must be known in order to adapt $R_\mathrm{s}$.

## VI. CONCLUSION

In this paper demands of the semiconductor industry for non-contaminative handling of agressive fluids at high temperatures are presented by showing the advantages of high temperatures for the photoresist stripping process. A bearingless pump that fulfills these demands is proposed.
The power, speed and torque requirements of the machine are approximated based on measurements taken from a low temperature pump. The torque and maximum current of the power electronics define the machine winding concept. This can then be used to calculate the losses in the machine. Based on this loss estimate it is shown how to calculate the heat distribution in the machine and how to optain the temperature at each winding layer. Ceramicly insulated nickel clad copper wire for the winding is chosen from two different wires to facilitate operation at the critical winding temperature of up tp $250\,°\mathrm{C}$. Finally, it is shown how to adapt the machine control to run the machine without hall sensors.

## REFERENCES

[1] R. Schöb, "Centrifugal pumps without bearing or seals," *World Pumps*, vol. 430, no. 12, pp. 34–37, 2002.
[2] X. Sun, L. Chen, and Z.Yang, "Overview of bearingless permanent-magnet synchronous motors," *Industrial Electronics, IEEE Transactions on*, vol. 60, no. 12, pp. 5528–5538, 2013.
[3] W. Gruber, S. Silber, W. Amrhein, and T. Nussbaumer, "Design variants of the bearingless segment motor," in *Power Electronics Electrical Drives Automation and Motion (SPEEDAM), 2010 International Symposium on*, pp. 1448–1453, June 2010.
[4] C. A. Mack, *Fundamental Principles of Optical Lithography: The Science of Microfabrication*. John Wiley & Sons, 2007.
[5] K. K. Christenson, J. W. Butterbaugh, T. J. Wagener, L. Nam, B. Schwab, M. Fussy, and J. Diedrick, "All wet stripping of implanted photoresist," *Solid State Phenomena*, vol. 134, pp. 109–113, 2007.
[6] R. Nan, F. Lee, J. Hung, J. M. Chu, J. Yuan, D. Yang, and J. W. Butterbauth, "Yield qualification of all wet photoresist stripping for cmos well loop implant masks in 300mm high volume manufacturing," *ECS Transactions*, vol. 25, no. 5, pp. 165–172, 2009.
[7] J. Sahiavo and R. Garber, "Air-operated high-temperature corrosive liquid pump," Mar. 23 1993. US Patent 5,195,878.
[8] J. Nerg, M. Rilla, and J. Pyrhonen, "Thermal analysis of radial-flux electrical machines with a high power density," *Industrial Electronics, IEEE Transactions on*, vol. 55, pp. 3543–3554, Oct 2008.
[9] V.-G. V. und Chemieingenieurwesen, *VDI Heat Atlas*. Springer reference, Springer, 2010.
[10] M. Jaritz and J. Biela, "Analytical model for the thermal resistance of windings consisting of solid or litz wire," in *Power Electronics and Applications (EPE), 2013 15th European Conference on*, pp. 1–10, Sept 2013.
[11] P. Karutz, T. Nussbaumer, and J. Kolar, "Magnetically levitated slice motors - an overview," in *Energy Conversion Congress and Exposition, 2009. ECCE 2009. IEEE*, pp. 1494–1501, Sept 2009.
[12] D. Steinert, T. Nussbaumer, and J. Kolar, "Slotless bearingless disk drive for high-speed and high-purity applications," *Industrial Electronics, IEEE Transactions on*, vol. 61, pp. 5974–5986, Nov 2014.
[13] K. Raggl, B. Warberger, T. Nussbaumer, S. Burger, and J. Kolar, "Robust angle-sensorless control of a pmsm bearingless pump," *Industrial Electronics, IEEE Transactions on*, vol. 56, pp. 2076–2085, June 2009.